

# Torus Formation in Neutron Star Mergers and GRB 050509b

R. Oechslin, H.-T. Janka

Max-Planck-Institut für Astrophysik, Karl-Schwarzschild-Str. 1, D-85741 Garching, Germany

## ABSTRACT

Merging neutron stars (NSs) are hot candidates for the still enigmatic sources of short gamma-ray bursts (GRBs). If the central engines of the huge energy release are accreting relic black holes (BHs) of such mergers, it is important to understand how the properties of the BH-torus systems, in particular disc masses and mass and rotation rate of the compact remnant, are linked to the characterizing parameters of the NS binaries. For this purpose we present relativistic smoothed particle hydrodynamics simulations with conformally flat approximation of the Einstein field equations and a physical, non-zero temperature equation of state. Disc formation is highlighted as a dynamical process caused by angular momentum transfer through tidal torques during the merging process of asymmetric systems or in the rapidly spinning triaxial post-merger object. Our simulations support the possibility that the first well-localized short and hard GRB 050509b has originated from a NS merger event. If so, its low energy output and short duration suggest that the merger remnant has collapsed to a BH within less than 100 ms, leaving an accretion torus with a small mass of  $< 0.01 M_{\odot}$ .

**Key words:** stars: neutron; gamma-rays: bursts; hydrodynamics; relativity; equation of state

## 1 INTRODUCTION

Merger events of NS+NS binaries do not only belong to the strongest known sources of gravitational wave (GW) radiation, they are also widely favored as origin of the class of short, hard GRBs (Blinnikov et al. 1984, Paczynski 1986, Eichler et al. 1989, Narayan et al. 1992). The recent first localization of a short burst, GRB 050509b, by Swift near a luminous, non-star-forming elliptical galaxy at redshift  $z = 0.225$  (Gehrels et al. 2005, Bloom et al. 2005) was interpreted as a possible first confirmation of this hypothesis (Bloom et al. 2005, Lee et al. 2005).

The central engines of such bursts are still poorly understood and observationally undetermined. But it seems unlikely that the energies required for typical short GRBs are set free during the dynamical phase of the merging of two NSs (Ruett et al. 1996). The production of GRBs by the neutrino emitting, hot post-merger NS is also disfavored, because the high mass loss rates caused by neutrino energy deposition near the NS surface rules out the production of high Lorentz factor outflow (Woosley & Baron 1992, Woosley 1993a). Instead, the long-time accretion of a BH formed from the transiently stable, hypermassive merger remnant (Morrison et al. 2004) is a much more promising source (e.g., Woosley 1993b, Ruett & Janka

1999, Popham, Woosley & Fryer 1999, Rosswog et al. 2003, Lee et al. 2005), provided the BH is surrounded by a sufficiently massive accretion torus. Due to the geometry of the BH-torus system with relatively baryon-poor regions along the rotation axis, thermal energy release preferentially above the poles of the BH by the annihilation of neutrino-antineutrino ( $\bar{\nu}\nu$ ) pairs (Jaroszynski 1993, Mochkovitch et al. 1993) can lead to collimated, highly relativistic jets of baryonic matter with properties in agreement with those needed to explain short GRBs (Abey et al. 2005). Alternatively or in addition, magnetic coupling between the rotating BH and the girding accretion torus could tap the rotational energy of the BH (Blindford & Znajek 1977) and could help powering magnetohydrodynamically (MHD)-driven outflow (e.g., Brown et al. 2000, Drachenhahn & Spruit 2002).

Torus mass as well as BH mass and rotation are thus crucial parameters that determine the energy release from the merger remnant on the secular timescale of the viscous evolution of the BH-torus system. In this letter we present a first set of results from new three-dimensional (3D), relativistic smoothed particle hydrodynamics simulations of NS mergers with a physical equation of state (EoS), which aim at establishing the link between the remnant properties and those of the binary sys-

tem s. Previous such attempts (see Baumgarte & Shapiro 2003 for a review) were either performed in the Newtonian limit (e.g., Ruett & Janka 2001 and references therein; Rosswog et al. 2003), or with polytropic or otherwise radically simplified treatment of the high- and low-density EoS and its temperature-dependent behaviour (e.g., Shibata, Taniguchi & Uryu 2003, Shibata et al. 2005), or considered disc formation by viscous (or magnetic) effects during the secular evolution of hypermassive NSs (Duez et al. 2004). Here we instead highlight torus formation in NS mergers as a dynamical process and argue that this is consistent with observations of GRB 050509b.

## 2 THE MODEL

We employ an improved version of our relativistic smoothed particle hydrodynamics (SPH) code (Oechslin et al. 2002, 2004), which solves the relativistic hydrodynamics equations together with the Einstein field equation in the conformally flat approximation (Isenberg & Nester 1980, Wilson, Mathews & Marronetti 1996). The code now allows for the use of a tabulated, non-zero temperature EoS and solves the energy equation in a form without explicit time derivatives of the metric elements on the RHS (cf. Oechslin et al. 2002, eqn. A8). The properties of the stellar plasma are described by the non-zero temperature EoS of Shen et al. (1998), which is used with baryonic density, internal energy and electron fraction as input and pressure and temperature as output. Since the backreaction of the neutrino emission on the stellar fluid is small on the timescales considered here, we ignore neutrinos in our models. As a consequence, the electron fraction  $Y_e$  needed by the EoS as an input remains constant in Lagrangian mass elements and is simply advected with the fluid.

We start our simulations shortly before the tidal instability sets in and follow the evolution with typically 400'000 SPH particles through merging and torus formation until either the collapse of the merger remnant sets in, or a quasi-stationary state has formed.

Initial conditions for our simulations are generated by placing two NSs in hydrostatic equilibrium on a circular orbit of a given orbital distance and by relaxing the configuration with the use of a small damping force into a circular orbital motion with an irrotational spin state. The orbital velocity is adjusted during this process in order to obtain the binary in orbital equilibrium. The initial electron fraction  $Y_e$  is obtained by requiring neutrinoless equilibrium for cold neutron stars after.

We consider a variety of models with different NS masses and mass ratios. Other unknown parameters like the NS spins and the EoS are kept fixed except for two models where thermal effects in the EoS are neglected. This is realized by reducing the EoS to the two-dimensional slice at  $T = 0$  with density and  $Y_e$  as input and pressure and internal energy as output. This reduction has no influence as long as shocks are absent, i.e. as long as the fluid evolves adiabatically. In the presence of shocks, however, the  $T = 0$  case corresponds to the extreme situation that a very efficient cooling mechanism extracts immediately the entropy and internal energy generated in shocks.

In Table 1, the key parameters characterizing our different

models are summarized. In the further analysis and discussion of our models, we have synchronized the time axis to the time of maximum gravitational wave luminosity. This allows for a better comparison of the temporal evolution.

## 3 RESULTS

### 3.1 Dynamics of merging

The evolution of a NS binary during the adiabatic inspiral is driven by gravitational radiation reaction. Once the binary becomes unstable to tidal forces, the hydrodynamic evolution sets in, leading to the tidal stretching of one or of both companions and to the formation of a central hypermassive NS surrounded by a thick, neutron-rich accretion torus. Depending on its mass and its rotation rate and the EoS, the hypermassive NS will collapse immediately or after a (short?) delay to a rapidly rotating BH (e.g. Morrison et al. 2004).

The dynamics and post-merging structure largely depend on the mass ratio  $q$  of the binary. In asymmetric systems with  $q$  significantly smaller than 1, the less massive but slightly larger star is tidally disrupted and deformed into an elongated primary spiral arm, which is mostly accreted onto the more massive companion. Its tail, however, contributes a major fraction to the subsequently forming thick disc/torus around a highly deformed and oscillating central remnant (see Fig. 6, panel (a)). In systems with  $q > 1$  and nearly equally sized stars, both stars are tidally stretched and directly plunge together into a deformed merger remnant (see Fig. 6, panel (d)). In all models, excited radial and non-radial oscillations of the compact remnant periodically lead to ejection of surface material into secondary tidal tails during the subsequent evolution. As illustrated in Fig. 6, this effect takes place both in symmetric and asymmetric cases, but is stronger in the latter because of the larger triaxial deformation of the post-merger object.

### 3.2 Disc Formation

If and when the compact post-merger object collapses to a BH (the secular evolution driven by GW radiation reaction, viscosity and MHD cannot be followed by 3D simulations), pressure support from the central remnant to the disc will vanish and matter will be prevented from infall mostly by rotational support. As a consequence, we distinguish future disc matter from the central remnant by demanding the specific angular momentum  $j$  to be larger than the one associated with the innermost stable circular orbit (ISCO) of a Kerr BH with the gravitational mass and the spin parameter of the central remnant.

The ISCO can be analytically determined in the case of the Boyer-Lindquist Kerr metric (Bardeen et al. 1972). In our case we shall use an approximate pseudo-Kerr metric (see, e.g., Grandclement et al. 2002) which is both isotropic and conformally flat, consistent with the coordinates we used for our numerical simulations. The ISCO can then be found among all circular orbits in the orbital plane by minimizing the specific angular momentum along the radial

Table 1. Parameters of the considered NS+NS models.  $M_1$  and  $M_2$  denote the individual gravitational masses of the NSs in isolation, while  $M_{\text{sum}} = M_1 + M_2$  stands for the sum of the two. Note that the total gravitational mass  $M$  is slightly smaller than  $M_{\text{sum}}$  because  $M$  also involves the negative gravitational binding energy between the two stars.  $M_0$  is the total baryonic mass,  $q = M_1/M_2$  and  $q_M = M_{0,1}/M_{0,2}$  are the gravitational and baryonic mass ratios, respectively. 'Shen' stands for the full, non-zero temperature EoS of Shen et al. (1998), while 'Shen\_c' denotes the  $T = 0$  slice of this EoS table. Characteristic data of the post-merger system are read off at  $t = 6$  ms.  $M_{0,\text{disc}}$  and  $J_{\text{disc}}$  are the baryonic mass and the angular momentum of the disc, respectively.  $M_{\text{rem}}$  is the remnant gravitational mass, and  $a_{\text{rem}} = (J_{\text{total}} - J_{\text{disc}})/M_{\text{rem}}^2$  is the corresponding spin parameter.  $j_{\text{ISCO}}$  and  $r_{\text{ISCO}}$  are the specific angular momentum and the radius of the ISCO of a Kerr-BH with the gravitational mass and spin parameter of the remnant.

| M odel  | $M_1$ | $M_2$ | $M_{\text{sum}}$ | $M_0$ | $q$  | $q_M$ | EoS    | $M_{0,\text{disc}}$ | $J_{\text{disc}}$                 | $M_{\text{rem}}$ | $a_{\text{rem}}$ | $j_{\text{ISCO}}$               | $r_{\text{ISCO}}$ |
|---------|-------|-------|------------------|-------|------|-------|--------|---------------------|-----------------------------------|------------------|------------------|---------------------------------|-------------------|
| Unit    | M     | M     | M                | M     |      |       |        | M                   | $10^{48} \text{ g cm}^2/\text{s}$ | M                |                  | $10^{16} \text{ cm}^2/\text{s}$ | km                |
| S1414   | 1.4   | 1.4   | 2.8              | 3.032 | 1.0  | 1.0   | Shen   | 0.02                | 1.49                              | 2.68             | 0.90             | 3.17                            | 11.8              |
| S138142 | 1.38  | 1.42  | 2.8              | 3.032 | 0.97 | 0.97  | Shen   | 0.02                | 1.93                              | 2.68             | 0.90             | 3.17                            | 11.8              |
| S135145 | 1.35  | 1.45  | 2.8              | 3.034 | 0.93 | 0.93  | Shen   | 0.04                | 3.42                              | 2.67             | 0.88             | 3.18                            | 11.9              |
| S1315   | 1.3   | 1.5   | 2.8              | 3.037 | 0.87 | 0.86  | Shen   | 0.08                | 6.84                              | 2.64             | 0.86             | 3.17                            | 11.9              |
| S1216   | 1.2   | 1.6   | 2.8              | 3.039 | 0.75 | 0.73  | Shen   | 0.15                | 12.10                             | 2.58             | 0.81             | 3.17                            | 12.1              |
| S1515   | 1.5   | 1.5   | 3.0              | 3.274 | 1.0  | 1.0   | Shen   | 0.01                | 1.75                              | 2.86             | 0.89             | 3.40                            | 12.6              |
| S1416   | 1.4   | 1.6   | 3.0              | 3.274 | 0.88 | 0.86  | Shen   | 0.06                | 4.39                              | 2.84             | 0.88             | 3.40                            | 12.7              |
| S1317   | 1.3   | 1.7   | 3.0              | 3.279 | 0.76 | 0.75  | Shen   | 0.13                | 10.79                             | 2.78             | 0.82             | 3.40                            | 12.8              |
| S1313   | 1.3   | 1.3   | 2.6              | 2.800 | 1.0  | 1.0   | Shen   | 0.03                | 2.19                              | 2.50             | 0.91             | 2.94                            | 10.9              |
| S1214   | 1.2   | 1.4   | 2.6              | 2.799 | 0.86 | 0.85  | Shen   | 0.11                | 8.59                              | 2.43             | 0.85             | 2.93                            | 10.9              |
| S1115   | 1.1   | 1.5   | 2.6              | 2.807 | 0.73 | 0.71  | Shen   | 0.17                | 13.24                             | 2.38             | 0.80             | 2.93                            | 11.1              |
| C1216   | 1.2   | 1.6   | 2.8              | 3.039 | 0.75 | 0.73  | Shen_c | 0.21                | 16.22                             | 2.48             | 0.79             | 3.06                            | 11.6              |
| C1315   | 1.3   | 1.5   | 2.8              | 3.037 | 0.87 | 0.86  | Shen_c | 0.14                | 10.61                             | 2.54             | 0.85             | 3.04                            | 11.5              |

coordinate.

Using this criterion, we are now able to identify the disc matter and disc mass for the various models considered. Their very different merger dynamics is reflected in the different evolution of the disc mass (see Fig. 1). The rapid rise in the asymmetric models around  $t' = 0$  ms can be associated with the development of the primary spiral arm. After this dynamical phase shortly after merging, a nearly stationary torus forms and the disc mass settles down to a slowly changing value, which is plotted versus mass ratio  $q$  for all models in Fig. 2. We find a roughly linear dependence with a flattening near  $q = 1$ . The disc mass rises from about  $0.02M$  at  $q = 1$  to about  $0.15M$  at  $q = 0.75$ . There is also a weaker inverse dependence of the disc mass on the total mass of the system (see Table 1).

We checked the consistency of our disc mass determination by comparing these masses to the amount of matter residing outside of  $r_{\text{ISCO}}$ , the ISCO radius. In all cases, we found  $M_{\text{gas}}(r > r_{\text{ISCO}}) > M_{\text{gas}}(j > j_{\text{ISCO}}) / M_{0,\text{disc}}$  by factors of two or more, suggesting that gas pressure still plays an important role in the quasi-stationary phase. Our disc masses are therefore lower limits, since pressure support will not completely vanish even after BH formation.

In Fig. 6 we have color-coded in red the material that belongs to the future disc, whereas the material that currently fulfills the disc mass criterion is shown in yellow. By definition, these two attributes coincide at the end of the simulation. We see that the future disc matter originates mainly from the spiral arm tips and from the stellar surface. This indicates that the formation of a post-merger disc is linked to the presence of spiral arms. Indeed, the yellow tips of these tidal tails in Fig. 6 and also the enhanced specific angular momentum in the outer edges of the tidal tails in Fig. 5 suggest angular momentum transfer from the central remnant to the spiral arm tips via tidal torques. This hypothesis is confirmed by a postprocessing analysis of model

C1216 where we integrated the torque exerted by gravitational and pressure forces from the compact remnant on the yellow mass elements in the primary spiral arm as a function of time. The result for the total angular momentum evolution agrees very well with the simulation result (Fig. 4).

An interesting effect can also be seen by comparing models with  $T = 0$  and  $T \neq 0$  EoSs. In Fig. 3 we show the disc mass evolution of the cold models C1216 and C1315 together with their non-zero temperature counterparts S1216 and S1315. Obviously, the first increase in disc mass, which can be associated with the cold primary spiral arm, is unaffected by temperature effects. Thermal pressure effects during the following evolution, however, reduce the further increase in disc mass in the non-zero temperature case, whereas in the cold case the disc mass increases by an additional  $0.07M$ . We determine two possible reasons for this difference. On the one hand, the core of the cold merger remnant contracts more strongly due to the absence of thermal pressure. Therefore, more gravitational binding energy is converted into rotational energy and the rotation rates become higher, supporting the formation of spiral arms. On the other hand, the shock-heated matter from the collision region between the two NSs forms a halo of hot matter which engulfs the compact remnant-torus system in the  $T \neq 0$  case. This halo may damp the oscillations of the remnant and the development of large deviations from axisymmetry.

#### 4 CONCLUSIONS

We have shown that nonradial oscillations and triaxial deformation and the associated tidal torques can mediate efficient angular momentum transfer in the compact remnant within the first milliseconds after the merging of two NSs. Applying different criteria, we estimated the mass of the torus which will survive the future collapse of the central, dense object

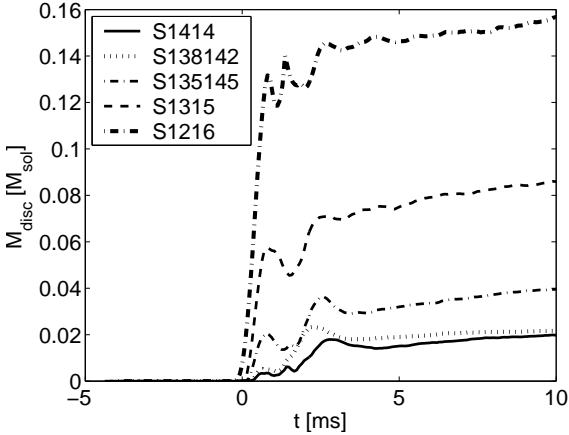


Figure 1. Disc formation in all models with non-zero temperature EoS used. Plotted is the disc mass as inferred from our disc mass criterion (see text). The final disc mass as given in Table 1 is read off at about 6 ms. Clearly visible is the rapid rise at  $t' = 0$ , which depends strongly on the mass ratio. On the other hand, the further evolution after merging is similar in all cases.

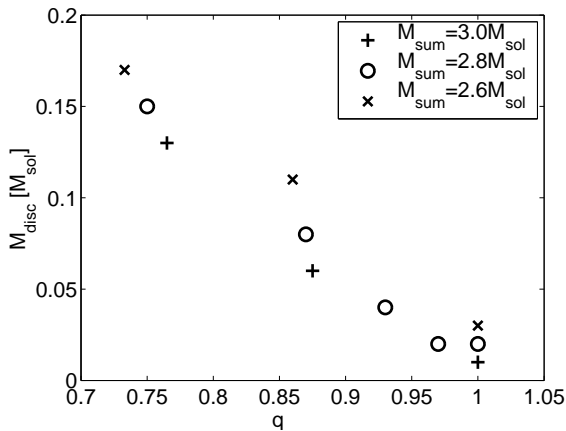


Figure 2. Disc masses versus mass ratio  $q$  for all non-zero temperature runs.

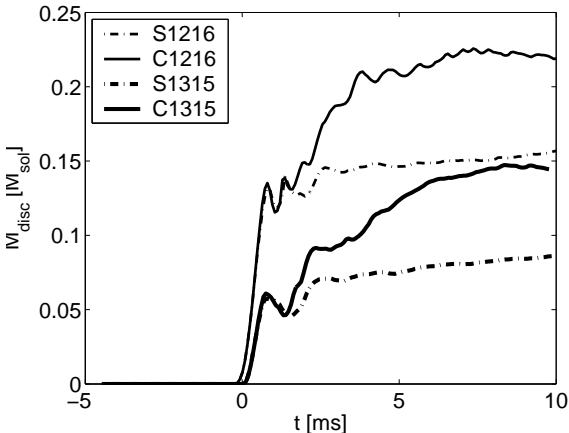


Figure 3. Same as in Fig. 1, but comparing the differences for  $T = 0$  and non-zero temperature EoSs.

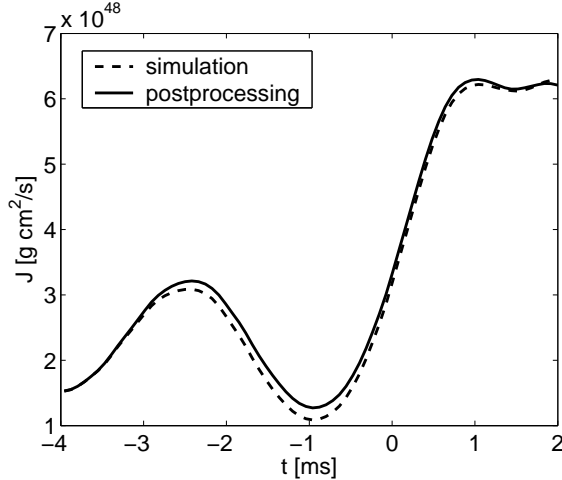


Figure 4. Total angular momentum for a blob of matter in the primary spiral arm of model C1216. The dashed line represents the results of the simulation, the solid line those of a postprocessing analysis.

to a BH. For the considered irrotational systems and the employed relatively stiff nuclear EoS of (Shen et al. 1998), we determined lower disc masses limits of  $< 1\%$  of the (baryonic) system mass for a NS-NS (gravitational) mass ratio around  $q = 1$ , increasing to about 6% for systems with  $q$  around 0.75. We observed also an inverse relation between torus mass and binary system mass (Fig. 2). These numbers include non-zero temperature effects, which turned out to be important and to reduce the disc mass by several 10% compared to the values for the  $T = 0$  case.

The disc masses obtained in our simulations concern the viability of post-merger BH-torus systems as central engines of short GRBs and annihilation as possible prime energy source at least in some cases. GRB 050509b, for example, has an intrinsic duration of  $t_{GRB} = 25$  ms and an isotropic energy of  $10^{48}$  erg if it is located at  $z = 0.225$  (Gehrels et al. 2005). Such a low-energy event can be explained by the accretion of discs in the lower range of masses found here for symmetric NS+NS binaries, even when conservative assumptions are made for the incompletely known efficiencies of the various processes between the energy release near the BH and the gamma-ray emission at  $10^{14}$  cm. Assuming that (1) about 5% of the accreted rest mass is radiated away by neutrinos (Lee et al. 2005, Setiawan et al. 2004), (2) about 1% of this energy is converted to an  $e^+e^-$ -pair plasma reball (Setiawan et al. 2004, Rueter & Janka 1999), (3) maybe only 10% of the reball energy is tapped for hydrodynamically accelerating baryonic outflow to ultrarelativistic velocities in jets (Aloy et al. 2005), (4) which are collimated into 1{10% of the sky ( $4 = \pi \cdot 10^2 M_{\odot}$ ; Aloy et al. 2005), and finally assuming (5) that less than 10% of the kinetic energy of these jets is dissipated in internal shocks and produces gamma-rays (e.g. Daigne & Mochkovitch 1998), one finds that an accreted mass of  $10^{-3}$  ( $10^{-2}$ )  $M_{\odot}$  is well sufficient to account for the energetics of GRB 050509b. Of course, similarly luminous GRBs at larger distances or with longer durations require more energy. But there are several degrees of freedom which may be exploited. Not only the disc masses are

much higher for asymmetric systems or systems in which the merging NSs possess spins. Also a softer nuclear EoS than used in our models might lead to larger torus masses. Moreover, since the compact proto-BHs found in our simulations have significant angular momentum ( $a_{\text{rem}}$  is between 0.8 and 0.93), the energy release in the accretion is likely to be boosted by Kerr effects and the Blandford-Znajek mechanism.

If further observations substantiate the link between NS+NS mergers and short GRBs, this may set constraints on the post-merging evolution and the nuclear EoS. On the one hand the hypermassive NS should escape the collapse to a BH for a sufficiently long time so that an accretion torus can form by the described dynamical process. On the other hand the collapse of the hot, neutrino radiating NS should not be delayed too much, because the neutrino luminosities obtained in NS+NS merger models (see Ruett & Janka 2001, Rosswog & Liebendorfer 2003) lead to a massive neutrino-driven wind (Woosley 1993a, Janka & Woosley 1996, Thompson et al. 2001). This non-relativistic wind will produce an extended baryonic halo around the future BH-torus system. A jet launched from such a system may sweep up so much mass from even a low-density and low-mass halo that the high Lorentz factor outflow needed for GRBs is efficiently prevented as shown in the type-A models of Alford et al. (2005). Similar to the collapsar scenario this obstacle can be overcome when the energy source provides a driving force for a timescale longer than the jet from the BH needs to reach the surface of the baryonic halo. This sets a limit to the lifetime of the hypermassive NS by the requirement that  $t_{\text{acc}} v_{\text{jet}} > R_{\text{wind}} = v_{\text{wind}} (t_{\text{BH}} + t_{\text{acc}})$ , where  $v_{\text{jet}} = c$  is the speed of the jet,  $R_{\text{wind}}$  the outer radius of the expanding halo,  $v_{\text{wind}}$  the corresponding wind expansion velocity,  $t_{\text{acc}}$  the timescale of torus accretion and energy release, and  $t_{\text{BH}}$  the BH formation timescale and thus the duration of the baryonic wind. For typical wind velocities of  $v_{\text{wind}} = 0.1c$  one finds  $t_{\text{BH}} < 9t_{\text{acc}}$ . Provided  $t_{\text{acc}} < t_{\text{GRB}}$  (Alford et al. 2005) this means that neutrino cooling and angular momentum redistribution and loss by non-axisymmetric hydrodynamic interaction and gravitational radiation (Shibata et al. 2005), or viscosity and MHD effects (Shapiro 2000) must have driven the hypermassive NS in GRB 050509b to gravitational instability on a timescale of  $< 200$  ms, implying that the merger remnant was closely above the maximum mass of stable, rigidly rotating NSs. The short accretion timescale also suggests that the torus mass was small, consistent with the conclusion drawn from the low energy of GRB 050509b and with the requirement from optical limits that little radiating material was ejected (Hjorth et al. 2005).

#### ACKNOWLEDGMENTS

We thank M. A. Alford for inspiring discussions and A. M. arek for preparing the EoS table used in this work. Support from the Sonderforschungsbereich-Transregio 7 of the Deutsche Forschungsgemeinschaft is acknowledged. The computations were performed at the Rechenzentrum Garching.

#### REFERENCES

Alford M. A., Janka H.-T., Müller E., 2005, *Astrophys. Astron.*, 243, 273

Bardeen J.M., Press W.H., Teukolsky S.A., 1972, *ApJ*, 178, 347

Baumgarte T.W., Shapiro S.L., 2003, *Phys. Rept.*, 376, 41

Blandford R.D., Znajek R.L., 1977, *MNRAS*, 179, 433

Blinnikov S.I., Novikov I.D., Perevodchikova T.V., Polnarev A.G., 1984, *Soviet Astron. Lett.*, 10, 177

Bloom, J.S. et al., 2005, subm. to *ApJ*, astro-ph/0505480

Brown et al., 2000, *New Astron.*, 5, 191

Daigne F., Mochkovitch R., 1998, *MNRAS*, 296, 275

Drenkhahn G., Spruit H.C., 2002, *Astrophys. Astrophys.*, 391, 1141

Duez M.D., Liu Y.T., Shapiro S.L., Stephens B.C., 2004, *Phys. Rev. D*, 69, 104030

Eichler D., Livio M., Piran T., Schramm D.N., 1989, *Nature*, 340, 126

Gehrels N. et al., submitted to *Nature*, astro-ph/0505630

Grandclément P., Gourgoulhon E., Bonazzola S., 2002, *Phys. Rev. D*, 65, 044021

Hjorth, J. et al., submitted to *ApJL*, astro-ph/0506123

Isenberg, J., Nester J., 1980, in *General Relativity and Gravitation*, Vol. 1, ed. A. Held, Plenum Press, New York (1980), p. 23

Jaroszynski M., 1993, *Acta Astron.*, 43, 183

Lee W.H., Ramirez-Ruiz E., Granot J., 2005, submitted to *ApJL*, astro-ph/0506104

Lee W.H., Ramirez-Ruiz E., Page D., 2005, to appear in *ApJ*, astro-ph/0506121

Mochkovitch R., Hernanz M., Isen J., Martin X., 1993, *Nature*, 361, 236

Morrison IA., Baumgarte T.W., Shapiro S.L., 2004, *ApJ*, 610, 941

Narayan R., Paczynski B., Piran T., 1992, *ApJ*, 395, L83

Oechslin R., Rosswog S., Thielemann F.K., 2002, *Phys. Rev. D*, 65, 103005

Oechslin R., Uryu K., Poghosyan G., Thielemann F.K., 2004, *MNRAS*, 349, 1469

Paczynski B., 1986, *ApJL*, 308, 43

Popham R., Woosley S.E., Fryer C., 1999, *ApJ*, 518, 356

Janka Y.-Z., Woosley S.E., 1996, *ApJ*, 518, 356

Rosswog S., Liebendorfer M., 2003, *MNRAS*, 342, 673

Rosswog S., Ramirez-Ruiz E., Davies M.B., 2003, *MNRAS*, 345, 1077

Ruett M., Janka H.-T., Schäfer, 1996, *Astrophys. Astrophys.*, 311, 532

Ruett M., Janka H.-T., 1999, *Astrophys. Astrophys.*, 344, 573

Ruett M., Janka H.-T., 2001, *Astrophys. Astrophys.*, 380, 544

Shapiro S.L., 2000, *ApJ*, 544, 397

Shen H., Toki H., Yamatsu K., Sumiyoshi K., 1998, *Nucl. Phys. A*, 637, 435

Setiawan S., Ruett M., Janka H.-T., 2004, *MNRAS*, 352, 753

Shibata M., Taniguchi K., Uryu K., 2003, *Phys. Rev. D*, 68, 084020

Shibata M., Taniguchi K., Uryu K., 2005, *Phys. Rev. D*, 71, 084021

Thompson T.A., Burrows A., Meyer B.S., 2001, *ApJ*, 562, 887

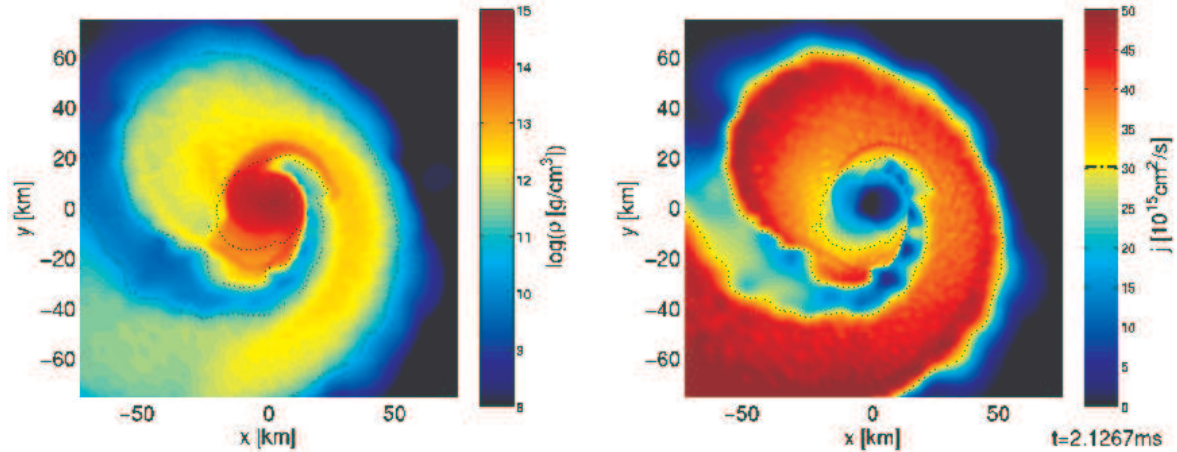


Figure 5. Model C1216: Density (left) and specific angular momentum distribution in the orbital plane. The black dotted line in both panels and in the right colorbar corresponds to the location where the specific angular momentum is equal to the value of  $j_{isco}$  at the given time (see text).

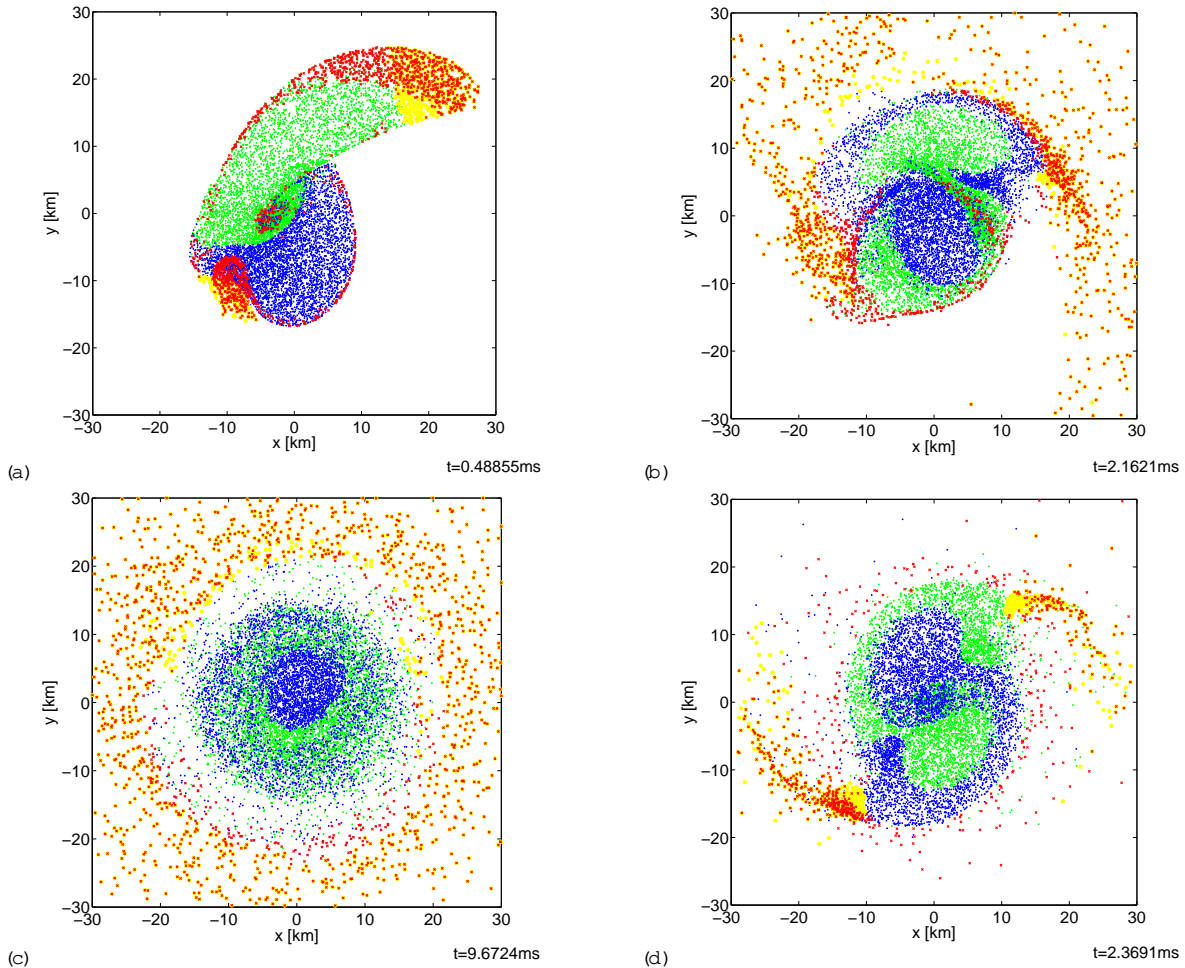


Figure 6. (a) Model C1216 during the merging phase with a primary spiral arm forming. Plotted is every 10th particle around the equatorial plane. The merger of the two stars is represented by green and blue particles, respectively. Particles that end up in the disc at the end of the simulation are marked in red and the ones that currently fulfill the disc criterion are plotted in yellow. (b) Same as (a), but 2 ms after merging when a secondary spiral arm appears. (c) Same as (a), but at the time when a quasi-stationary torus has formed. Note that the particle density is not strictly proportional to the density of the uid because the particles near the initial stellar boundaries are attributed a smaller particle mass. These particles preferentially end up in the torus so that the particle density there appears enlarged. (d) Same as (a) but for Model S1414. The primary spiral arm is absent in the symmetric binary case and the post-merging (secondary) arms are smaller than in the asymmetric models.

Wilson J.R., Matthews G.J., Maronetti P., 1996, Phys.

Rev. D, 54, 1317

Woolley S.E., Baron E., 1992, ApJ, 391, 228

Woolley, S.E., 1993a, Astron. Astrophys. Suppl., 97, 205

Woolley, S.E., 1993b, ApJ, 405, 273